refraction data from all continents would define the constants of equation (3) more precisely, and allow altitude anomalies to be mapped over the whole Earth.

I interpret variation in crustal thickness as being mainly due to two effects. (1) Because surface altitude and mean crustal density vary relatively rapidly on continents, the crust appears to be in isostatic equilibrium with an upper mantle of uniform density, so variation in surface altitude and mean crustal density show a strong correlation with variation in mean crustal thickness. (2) Isostatic equilibrium is actually between the whole lithosphere and the asthenosphere[13], so, to keep equal pressure on the asthenosphere and keep the continental crust near sea level, any regional variation in lower lithosphere density causes regional variation in continental crustal thickness.

This work is published with the permission of the Director, Bureau of Mineral Resources, Canberra.

Received 17 March; accepted 29 June 1982.

1. Cochran, J. R. & Talwani, M. *Geophys. J. R. astr. Soc.* **50**, 495–522 (1977).
2. Woollard, G. P. *Phys. Earth planet. Inter.* **3**, 484–498 (1970).
3. Talwani, M., Sutton, G. H. & Worzel, J. O. *J. geophys. Res.* **64**, 1545–1555 (1959).
4. Drummond, B. J., Smith, R. E. & Horwitz, R. C. *Geol. Soc. Aust. Spec. Publ.* **7**, 33–41 (1981).
5. Wellman, P. *BMR J. Aust. J. Geol. Geophys.* **1**, 297–302 (1976); **3**, 153–162 (1978); **4**, 373–382 (1979).
6. Manghnani, M. H., Ramananantoandro, R. & Clark, S. P. *J. geophys. Res.* **79**, 4527–5446 (1974).
7. Drummond, B. J. & Shelley, H. M. *BMR J. Aust. Geol. Geophys.* **6**, 137–143 (1981).
8. Cleary, J. *Bull. seis. Soc. Am.* **57**, 773–781 (1967).
9. Everingham, I. B. *Bur. Min. Resourc. Aust. Rec.* 1969/22 (1969).
10. Cleary, J. R., Simpson, D. W. & Muirhead, K. J. *Nature* **236**, 111–112 (1972).
11. Cull, J. P. *BMR J. Aust. Geol. Geophys.* **7**, 11–21 (1982).
12. Jordan, T. H. *Nature* **274**, 554–548 (1978).
13. Dooley, J. C. *BMR J. Aust. Geol. Geophys.* **2**, 1–5 (1977).
14. Cleary, J. R. *Tectonophysics* **20**, 241–248 (1973).
15. Finlayson, D. M. *J. geol. Soc. Aust.* **15**, 35–50 (1968).
16. Mathur, S. P. *Tectonophysics* **24**, 151–182 (1974).
17. Collins, C. D. N. *BMR J. Aust. Geol. Geophys.* **3**, 203–209 (1978).
18. Shackleford, P. R. J. & Sutton, D. J. *J. geol. Soc. Aust.* **28**, 491–500 (1981).
19. Finlayson, D. M., Collins, C. D. N. & Denham, D. *Phys. Earth planet. Inter.* **21**, 321–342 (1980).
20. Finlayson, D. M., Prodehl, C. & Collins, C. D. N. *BMR J. Aust. Geol. Geophys.* **4**, 243–252 (1979).
21. Finlayson, D. M. & McCracken, H. M. *J. geol. Soc. Aust.* **28**, 177–190 (1981).
22. Drummond, B. J. *BMR J. Aust. Geol. Geophys.* **4**, 171–180 (1979).
23. Drummond, B. J. *BMR J. Geol. Geophys.* **6**, 123–135 (1981).
24. Finlayson, D. M. *J. geophys. Res.* (in the press).
25. Collins, C. D. N. *BMR J. Aust. Geol. Geophys.* (in the press).
26. Jacobson, R. S., Shor, G. G., Kieckhefer, R. M. & Purdy, G. M. *Am. Ass. petrol. Geol. Mem.* **29**, 209–222 (1979).
27. Rynn, J. M. W. & Reid, I. D. *J. geol. Soc. Aust.* (in the press).

Vertical distribution and isotopic fractionation of living planktonic foraminifera from the Panama Basin

Richard G. Fairbanks*, Marc Sverdlove*, Rosemary Free*, Peter H. Wiebe† & Allan W. H. Bé*

* Lamont-Doherty Geological Observatory of Columbia University, Palisades, New York 10964, USA
† Woods Hole Oceanographic Institution, Woods Hole, Massachusetts 02543, USA

A model[1,2], which explains the vertical and seasonal distribution of planktonic foraminifera was developed using data from the western North Atlantic and is comprised of three tenets: (1) The conditions in the photic zone (upper 80–100 m) exclusively dictate planktonic foraminifera species composition and abundance throughout the water column. (2) Species are vertically stratified within the photic zone according to their temperature preference. Depth distribution according to temperature preference has been proposed by several authors[3] based on isotope analyses of sediments. Due to seasonal temperature variations, seasonal variations in the $\delta^{18}O$ composition of seawater, and species-specific isotope fractionation, rigorous proof of this hypothesis cannot be provided from sediment analyses alone. (3) The chlorophyll maximum is a major food source zone, which is preferentially exploited by foraminifera. Our data from the Panama Basin, which are presented here, are confirmation of this model. The Panama Basin in the eastern equatorial Pacific, which has a shallow and steep thermocline, was sampled for living planktonic foraminifera. A multiple opening–closing net and environmental sensing system (MOCNESS)[4] was used to collect 13 sets of eight vertically stratified oblique samples. We report here the quantitative distribution and stable isotopic composition of planktonic foraminifera from four MOCNESS tows taken over 5 days, during August 1979 (RV *Knorr* cruise 73) at 5°20′ N, 8°50′ W. Each tow consisted of eight samples which integrated ~12.5-m intervals from 0 to 100 m for MOC 126, 25-m intervals from 0 to 200 m for MOC 127, 100–150-m intervals from 0 to 1,000 m on MOC 128 and 250-m intervals from 0 to 2,000 m on MOC 131.

Oxygen and carbon isotope analyses were made on planktonic foraminifera from the MOCNESS tows and the surrounding seawater. Isotope determinations were made on a triple collector mass spectrometer (Micromass 903). The carbonate samples were vacuum roasted at 375 °C for 1 h and reacted with 100% phosphoric acid at 50 °C. The precision for carbonate is ±0.05‰ for oxygen and carbon. The $\delta^{18}O$ composition of seawater was determined with a rapid equilibration-extraction method described in ref. 5. The $\delta^{13}C$ composition of total dissolved CO_2 was predicted using the PO_4–$\delta^{13}C$ relationship given in ref. 6 and PO_4 data for a station occupied in between MOCNESS tows. The 0–100-m series provided an ideal test of the previous model[1,2] for several reasons. (1) Eight MOCNESS oblique tows at 12.5-m intervals (MOC 126) provide high resolution sampling. (2) There is a 15 °C temperature gradient in the upper 100 m, encompassing one of the steepest thermoclines (0.5 °C m^{-1}) in the world's oceans which occurs between 25 and 37.5 m. (3) The region is extremely productive, and foraminifera are abundant. (4) A sharp chlorophyll maximum is well developed in the thermocline[7]. (5) The water column was sampled for measurement of $\delta^{18}O$ of seawater.

Twenty-three species of planktonic foraminifera were identified in the Panama Basin tows. In the 0–100-m tow, MOC 126 (Fig. 1*a*), 16 species averaged more than 10 per 1,000 m^3. The dominant species, *Globoquadrina dutertrei*, showed a pronounced abundance peak between 25 and 50 m, precisely the interval corresponding to the steep thermocline, highest primary productivity and the associated deep chlorophyll maximum (DCM) (Fig. 1*a*)[7]. Nine out of 16 species or morphotypes showed pronounced maxima in the steep thermocline. Note that the abundance axis is logarithmic. *Globigerinoides sacculifer* and *Globigerinoides conglobatus* were numerically dominant at the chlorophyll maximum, but they showed comparable abundances in the surface mixed layer. *Globigerinoides ruber*, *Globigerinita glutinata*, *G. sacculifer* (without final sac chamber), and *G. conglobatus* were very abundant in the less productive surface mixed layer. Two species which secrete morphologically distinct terminal chambers. *Orbulina universa* and *G. sacculifer*, showed sharp maximum concentrations of these morphologies in the chlorophyll maximum zone between 25 and 37 m (Fig. 1*a*). *Globigerina calida* and *Globorotalia theyeri* had maxima below the steep thermocline. Of particular significance is the observation that the *G. theyeri* population descended from a maximum at 100 m on 4 August, MOC 127 (Fig. 1*b*) to between 250 and 375 m on 5 August, MOC 128 (Fig. 1*c*) to a maximum between 500 and 750 m on 8 August, MOC 131 (Fig. 1*d*). This averaged to a 170 m per day descent rate.

Oxygen isotope measurements of seawater (Fig. 2) and continuous temperature and conductivity measurements during the MOCNESS tows permit the construction of an accurate calcite

0028–0836/82/340841—04$01.00

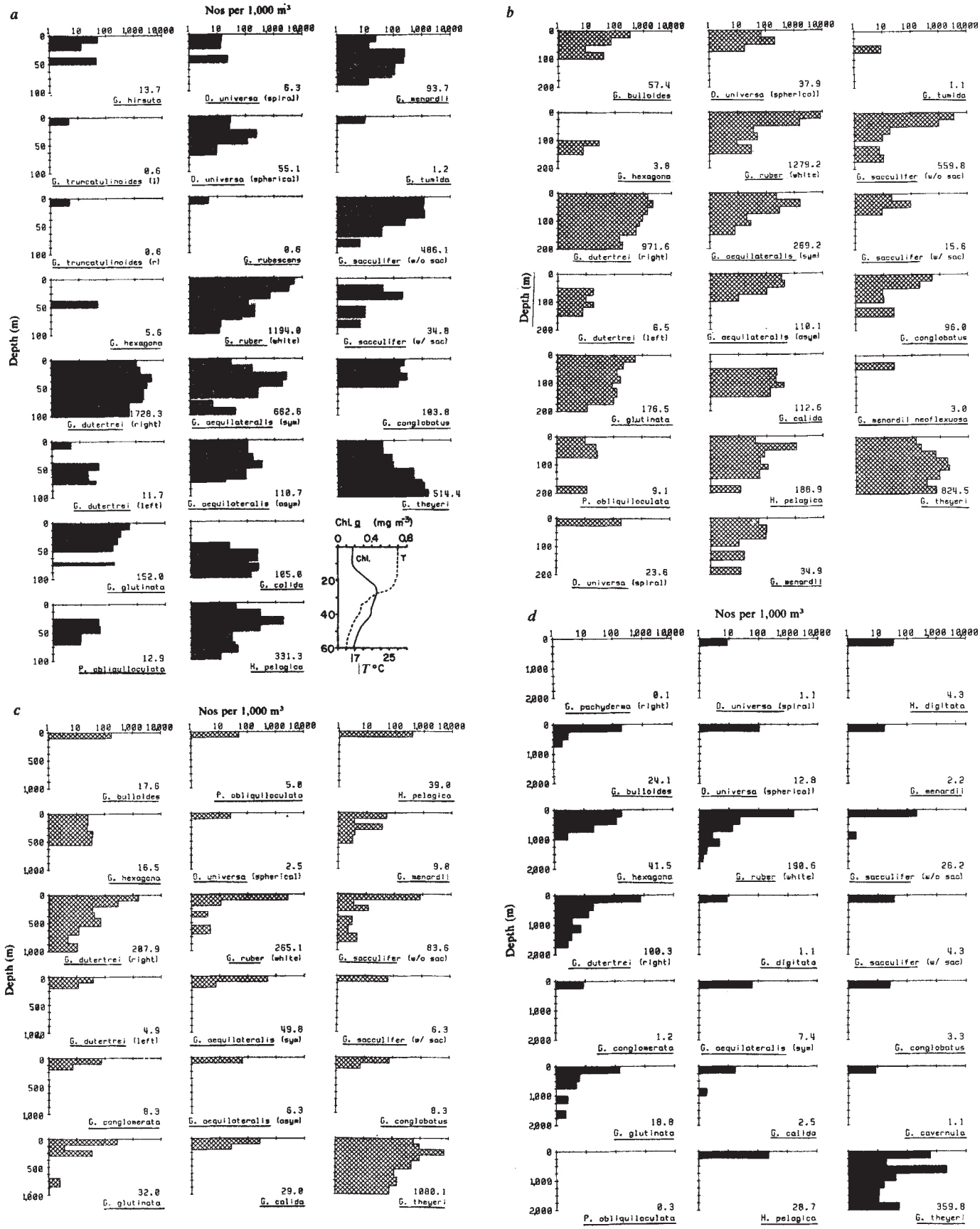

Fig. 1 *a*, Vertical profiles of living planktonic foraminifera caught in MOCNESS 126 oblique hauls in the Panama Basin between 0 and 100 m (3 August 1979; night). The number in the lower right corner of each histogram represents the average number per 1,000 m^3 over the interval towed, in this case 0–100 m. Temperature and chlorophyll profiles for this station are in the lower right corner. Chlorophyll data from Marra *et al.*[7]. *b*, Vertical profiles of living planktonic foraminifera caught in MOCNESS 127 oblique hauls in the Panama Basin between 0 and 200 m (4 August 1979; day). *c*, Vertical profiles of living planktonic foraminifera caught in MOCNESS 128 oblique hauls in the Panama Basin between 0 and 1,000 m (5 August 1979; day). *d*, Vertical profiles of living planktonic foraminifera caught in MOCNESS 131 oblique hauls in the Panama Basin between 0 and 2,000 m (8 August 1979; night).

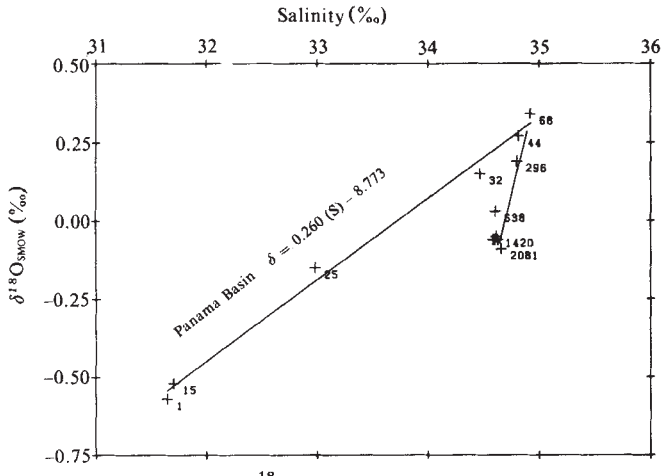

Fig. 2 Salinity versus $\delta^{18}O_{SMOW}$ for the Panama Basin. The numbers next to the symbols indicate water depth. The data indicate binary mixing between surface water and intermediate water, and deep water and intermediate water.

equilibrium profile (Fig. 3*a*) using the mollusc equation of Epstein *et al.*[8]. Oxygen isotope measurements of several different size fractions of nine foraminifera species or morphotypes show that shell growth is restricted to the upper 100 m, even though many species are found in abundance below 100 m. The oxygen isotope data indicate that specimens found below 100 m were simply descending through the water column while adding little or no additional calcite (Fig. 3*a*). It is also evident from the $\delta^{18}O$ versus depth plots (Fig. 3*a*) that most species generally grow within narrower depth intervals within the photic zone than their overall distribution would imply. For example, *G. ruber* is found in decreasing numbers between the surface and 100 m (Fig. 1*a*). Its $\delta^{18}O$ composition indicates that it is growing typically 0.5‰ lighter than equilibrium[1,2,9] in the surface mixed layer. Between 25 and 37.5 m *G. ruber* is adding some calcite, but below this level the data-point at 60 m indicates vertical descent from the mixed-layer.

G. dutertrei calcifies in oxygen isotope equilibrium[2] and the isotope data indicate growth in the thermocline, where *G. dutertrei* are found in maximum abundance (Fig. 1*a*). Between 37.5 and 100 m, *G. dutertrei* becomes only slightly enriched in $\delta^{18}O$, and are far from equilibrium at these depths. This is evidence that they are descending from the steep thermocline (Fig. 3*a*). The slight $\delta^{18}O$ enrichment is probably due to shell thickening[2,3]. Scanning electron microscope observations are needed to confirm this hypothesis.

G. theyeri and *G. calida* appear to be in oxygen isotopic equilibrium between 50 and 100 m, where they are dominant in MOC 126 and MOC 127, but their isotopic values do not change when they are collected below the photic zone (approximately upper 100 m) even though they may be numerically dominant below 100 m. Again, vertical descent is obvious and, in these two examples, no additional calcite was added during descent, otherwise we would observe a shift towards the equilibrium line. Thus we feel confident that this sampling strategy adequately captures all adult stages of shell calcification and allows us to examine the entire calcification process.

There is a 2‰ decrease in the $\delta^{13}C$ of total dissolved CO_2 between the surface and 100 m at the site of MOC 126 (Fig. 3*b*). There is some evidence that the $\delta^{13}C$ compositions of *G. dutertrei* and *Globigerinella aequilateralis* are affected by this gradient. *G. dutertrei* decreases more than 1‰ $\delta^{13}C$ between the surface and 100 m (Fig. 3*b*). The largest drop in $\delta^{13}C$ for *G. dutertrei* is coincident with the 1.5‰ decrease in $\delta^{13}C$ of total dissolved CO_2 in the steep thermocline. *G. aequilateralis* show a less significant shift in $\delta^{13}C$, but this species also parallels the seawater trend. The carbon isotope equilibrium line for inorganic calcite would fall to the right of the data, but parallel to the $\delta^{13}C$ of total dissolved CO_2 line (see ref. 9 for a discussion of calcite isotope equilibrium).

Note that *G. dutertrei* and *G. theyeri*, which calcify in oxygen isotope equilibrium, have the same carbon isotopic composition as ambient $\delta^{13}C$ of total dissolved CO_2 (Fig. 3*b*). As noted above, oxygen isotope measurements of *G. dutertrei* indicate equilibrium precipitation at ~30 m (Fig. 3*b*). Below 30 m *G. dutertrei* shows oxygen isotope enrichment, but the data are

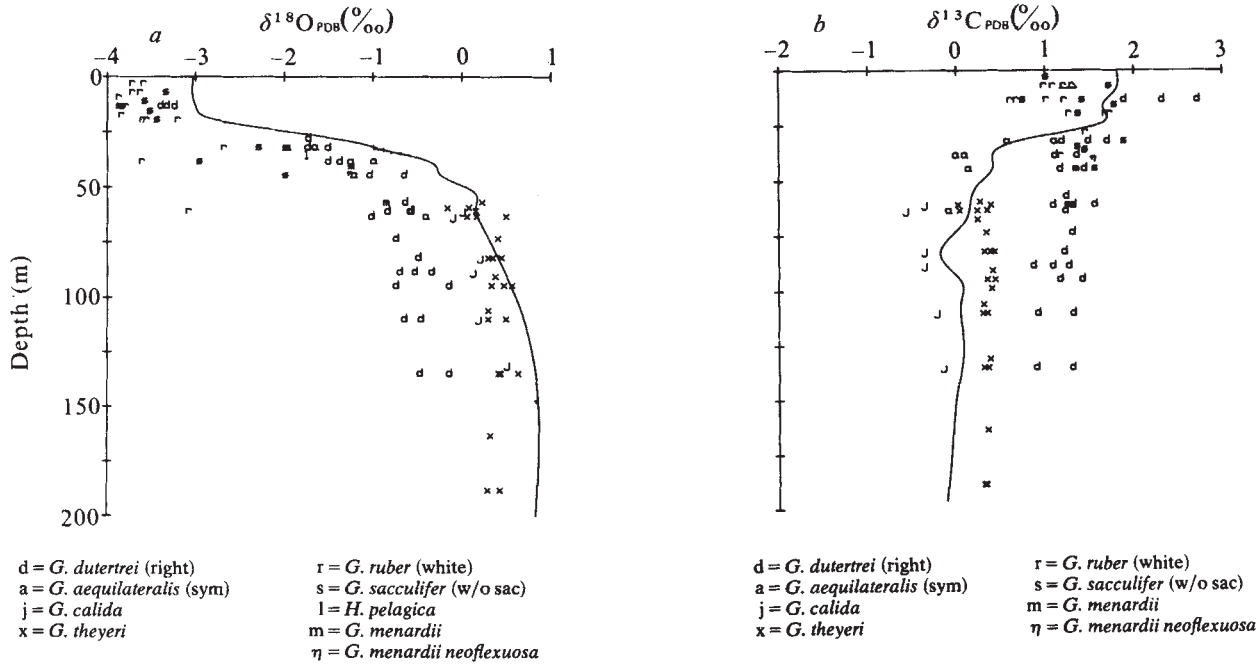

Fig. 3 *a*, Oxygen isotope composition of various size fractions of planktonic foraminifera as a function of depth in MOC 126, 0–100 m and MOC 127, 0–200 m. The solid line is the calculated equilibrium $CaCO_3$–$\delta^{18}O$ variation. All specimens plotted were protoplasm full. Corresponds to histograms in Fig. 1*a*, *b*. Carbon isotope composition of various size fractions of planktonic foraminifera as a function of depth in MOC 126, 0–100 m and MOC 127, 0–200 m. The solid line is the $\delta^{13}C$ of total dissolved CO_2.

significantly lighter than equilibrium, indicating vertical descent from 30 m. Similarly *G. dutertrei* calcite has the same $\delta^{13}C$ as the $\delta^{13}C$ of total CO_2 at 30 m and shows departure from the $\delta^{13}C$ of total CO_2 curve below 30 m, which is in agreement with the $\delta^{18}O$ data. *G. theyeri* is in oxygen isotope equilibrium between 50 and 75 m and also has the same $\delta^{13}C$ of carbonate as ambient $\delta^{13}C$ of total dissolved CO_2. *G. theyeri* differs from *G. dutertrei* by 1‰. The algal symbiont bearing species (such as *G. ruber, G. sacculifer, G. aequilateralis*) are generally depleted with respect to ^{13}C when compared with the ambient $\delta^{13}C$ of total dissolved CO_2.

We thank Greg Kolibas for stable isotope measurements, Ted Baker for computer programming and J. K. Bishop for providing PO_4 data. Contribution no. 3358 from Lamont-Doherty Geological Observatory of Columbia University and contribution no. 5139 from the Woods Hole Oceanographic Institution. This work was supported by NSF grant OCE 7725976 (R.G.F.) and ONR grants N00014-750210 and N00014-800098.

Received 25 March; accepted 24 May 1982.

1. Fairbanks, R. G. & Wiebe, P. H. *Science* **209,** 1524 (1980).
2. Fairbanks, R. G., Wiebe, P. H. & Bé, A. W. *Science* **207,** 61 (1980).
3. Emiliani, C. *Am. J. Sci.* **252,** 149 (1954).
4. Wiebe, P. H., Burt, K. H., Boyd, S. H. & Morton, A. W. *J. mar. Res.* **34,** 313 (1976).
5. Fairbanks, R. G. *J. geophys. Res.* **87,** 5796 (1982).
6. Broecker,, W. S. *Prog. Oceanog.* **11,** 151 (1982).
7. Marra, J. Wiebe, P. H., Stepien, J. C. & Bishop, J. K. (in preparation).
8. Epstein, S., Bucksbaum, R., Lowenstam, H. A. & Urey, H. C. *Bull. geol. Soc. Am.* **64,** 1315 (1953).
9. Williams, D. F., Bé, A. W. H. & Fairbanks, R. G. *Science* **206,** 447 (1979).
10. Turner, J. V. (in preparation).

Trans-sexually grafted antennae influence development of sexually dimorphic neurones in moth brain

Anne M. Schneiderman*‡, Steven G. Matsumoto* & John G. Hildebrand†

* Department of Neurobiology, Harvard Medical School, Boston, Massachusetts 02115, USA
† Department of Biological Sciences, Columbia University, New York, New York 10027, USA

Observations in insects reveal sexual differences in the central nervous system (CNS), associated with sexually dimorphic patterns of reproductive behaviour[1–9]. For example, in certain species of moths, including the sphinx moth *Manduca sexta*, only males fly towards a sexually receptive female or towards a source of the female sex pheromone[10,11]. In *Manduca*, specialized olfactory receptor cells found only on male antennae[12,13] respond sensitively and selectively to the female sex pheromone (unpublished experiments with K.-E. Kaissling and R. J. O'Connell). Their axons project into the macroglomerular complex (MGC), which is characteristic of male, but not female, antennal lobes (ALs; Fig. 1*b, d*)[1–3,5,8,9,14]. These afferents to the MGC presumably synapse with male-specific AL neurones[8,15] to begin the processing of phenomonal information. We have now devised a surgical procedure for producing antennal gynandromorphs of *Manduca* in which one of the two ALs receives sensory innervation from an antenna formed by a transplanted imaginal disk of the opposite sex. We report here that in these gynandromorphs, the physiological and morphological properties of certain AL neurones are influenced by the gender of the antennal sensory axons contacting them. In particular, neurones resembling the male-specific AL neurones appear in female ALs innervated by sensory axons from a grafted male antenna.

We produced 329 gynandromorphic larvae (Table 1, group 1), of which 78% metamorphosed and eclosed as adult moths. In 49% of these moths, the transplanted imaginal disk had everted and formed an antenna. All transplanted antennae exhibited structure characteristic of the donor's sex; none appeared to be modified by transplantation into a host of the opposite sex.

In 59% of the animals with everted grafts, the AL on the operated side was innervated by the nerve from the transplanted antenna. In these animals, the ingrowing sensory axons found their targets, the AL neurones, even though the pupal antennal nerve, comprising axons believed to provide contact guidance for antennal afferents[13,16], had been severed during surgery. We presume that the axons followed stumps of the 'guide fibres' still associated with the AL and suspect that the growing axons failed to do so in the remaining animals (41% of those with everted grafts). In the latter, the antennal nerve either ended abruptly as a mass of fibres near the base of the antenna or grew into the lateral protocerebrum, proboscis, or sub-oesophageal ganglion. In these animals, the operated AL was stunted, as in the deafferented AL in a deantennated moth[17,18]. No innervation of the contralateral AL by the graft was ever observed.

We examined histological sections from the brains of unoperated moths and antennal gynandromorphs (Fig. 1; Table 1,

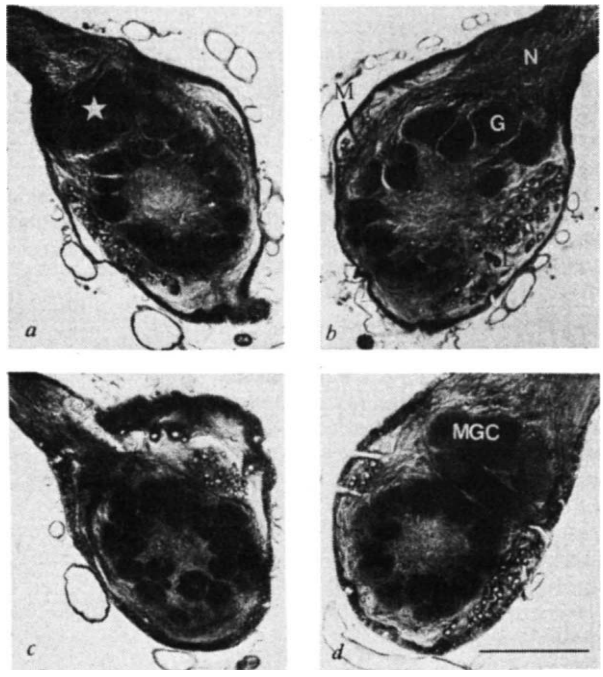

Fig. 1 Frontal sections through the operated (gynandromorphic) and control (normal) ALs of female (*a, b*) and male (*c, d*) moths, prepared from paraffin-embedded preparations and stained with Cresylecht violet and Luxol fast blue[18]. To produce antennal gynandromorphs of *Manduca*, antennal disks are transplanted unilaterally on the first or second day of the fifth (last) larval instar. Larvae are restrained in aluminium tubes and anaesthetized by chilling in a bath of ice-cold water. The antennal disk[14], which lies within the head capsule near the base of the larval antenna, is excised and replaced with the corresponding disk from a donor of the opposite sex. A mixture of phenylthiourea, streptomycin sulphate and penicillin (2:1:1)[19] is placed in the wound, which is then sealed by melted myristic acid (W. Harris, personal communication). In *b*, the antennal nerve (N) enters the normal female AL. The glomeruli (G) are arrayed around a central region of coarser neuropil. The cell bodies of the AL neurones are gathered in three cortical groups: a large lateral cluster (L), a smaller medial cluster (M) and a small group anterior to this plane of section. The normal male AL (*d*) characteristically exhibits the MGC, which lies near the entrance of the antennal nerve and is not present in the normal female AL (*b*). In the gynandromorphic female AL (*a*), a structure resembling the MGC (☆) lies near the entrance of the antennal nerve from the grafted male antenna. The gynandromorphic male AL (*c*) lacks a MGC. Scale bar, 200 μm.

‡ Present address: Department of Biological Sciences, 901 Fairchild, Columbia University, New York, New York 10027, USA.

0028-0836/82/340844—03$01.00